A Biomechanical Analysis Framework for Co-Correlation of 7T MR Elastography Measures and Amyloid Beta Deposition

Emily Triolo[1], Mackenzie Langan[2,3], Oleksandr Khegai[2], Akbar Alipour[2], Carolina Ferreira-Atuesta[3], Aymeric Pionteck[1], Jonathan Sutkowski[3], Trey Hedden[3], Priti Balchandani[2], and Mehmet Kurt[1,2]
[1]Mechanical Engineering, University of Washington, Seattle, WA, United States, [2]Biomedical Engineering and Imaging Institute, Ichan School of Medicine at Mount Sinai, New York City, NY, United States, [3]Graduate School of Biomedical Sciences, Ichan School of Medicine at Mount Sinai, New York City, NY, United States

Synopsis

Previous studies have implied the future use of MRE metrics to track disease progression and as a tool for AD diagnosis, potentially replacing or augmenting methods that use ionizing radiation. In this pilot study, we have therefore developed a novel framework for performing ultrahigh field (7T) MRE at high resolution on subjects who have previously undergone PET scans and performing joint analysis of biomechanical and pathologic markers on these subjects. We have successfully created a framework for measurement of high-resolution brain mechanical properties for co-correlation with traditional PET measures to be used on AD patients in the future.

Introduction

Alzheimer's disease (AD) is a neurodegenerative disease caused by abnormal deposits of amyloid plaques and intracellular neurofibrillary tangles of the protein tau[1]. Damage is initially found in the hippocampus and entorhinal cortex, where the connections between neurons are lost and those neurons die over time[2]. Over the progression of AD, the damage spreads throughout the brain, shrinking the volume of the overall brain tissue. Symptoms include memory loss, confusion, and cognitive difficulties. Early diagnosis of AD is still challenging because of the subtlety of the microstructural changes it initially causes in the brain, which is particularly troubling, as most treatments for AD can only be used to slow its progression, not reverse it, and are often far more successful when started early. Pivotal studies applying MRE have shown a progressive softening of white and gray matter tissue in AD patients compared to healthy controls (especially in the frontal, parietal and temporal lobes) in line with the known topography of AD pathology[3,4]. This implies the future use of MRI and MRE metrics to track disease progression and as a tool for AD diagnosis, potentially replacing methods that require patients to undergo ionizing radiation on a regular basis.

Although MRE studies on AD patients have identified tissue softening, there might be different spatiotemporal effects of tau and amyloid beta on brain tissue mechanics due to the intracellular and extracellular nature of their deposition. There might be competing effects of tissue atrophy and plaque formation on the measured brain mechanical properties. Therefore, one of the limitations of using MRE on AD patients is the lack of understanding of microstructural causes that induce tissue viscoelasticity variations. This difficulty limits the current predictive value of MRE for early diagnosis and for the assessment of individual risk of developing cognitive decline. To overcome this challenge, in this pilot study, we developed a novel framework for performing 7T MRE at high resolution on subjects who have previously undergone PET scans, and performing joint analysis of biomechanical and pathologic markers on these subjects. This approach has the potential to provide physical understanding regarding the meaning of these MRE parameters in the context of dementia and neurodegeneration.

Methods

Full brain coverage MRE (using a custom SE-2D-EPI-based sequence[5]) was performed on six healthy human subjects (Avg. age 73.2 years) at 1.1mm isotropic resolution and 50Hz vibration frequency[6], using a 32-channel head coil (Nova Medical) on a 7T Siemens Magnetom MRI scanner (TR/slice=140ms, TE=65ms, GRAPPA=3, Partial Fourier 7/8). Raw data were collected for each of these scanning sessions, and images were reconstructed post-hoc using Gadgetron to reduce the occurrence of phase singularities often found in standard reconstructions of this type. Images were denoised using a MP-PCA algorithm[5] and unwrapped using Segue 4D unwrapping[7]. Curl filtering, Fourier decomposition, and a quartic smoothing kernel[7] were used to acquire wavefield images, before Algebraic Inversion of the Helmholtz Equation was used to calculate the complex shear stiffness[8] (Figure 1). T1 images were segmented using Freesurfer and co-registered to the magnitude images of the MRE acquisition such that a transformation matrix was generated. This transformation matrix was then applied to the masks to be directly applied to the calculated elastograms.

These six subjects have also previously undergone a Aβ burden measurement with F18–labeled florbetaben simultaneous positron emission tomography and magnetic resonance (PET-MR) imaging on a Siemens Biograph mMR using standardized protocols in accordance with FDA labeling instructions. Attenuation-corrected data from 90-110 minute post-injection are measured in 1-minute windows and corrected for motion. PET data are expressed as a selective uptake value (SUV) (Figure 1). These PET images were also co-registered to the T1 images captured during the 7T MRI scanning session and previously generated Freesurfer masks applied.

Results

Using 7T neuroimaging and advanced signal processing techniques, we have successfully created a framework for measurement of high-resolution brain mechanical properties. Average Loss Modulus, Storage Modulus, and SUVR for each brain region for each subject was calculated and can be found listed in Table 1. A regression for each brain region between average SUVR and average Loss and Storage Modulus was also performed. The correlation coefficients and p-values for each brain region can be found in Table 2.

Discussion

Based on these correlation coefficients, for healthy older adults, there is a strong positive correlation between SUVR and Storage Modulus that is approaching significance in the Entorhinal cortex, as well as a strong positive correlation between SUVR and Storage Modulus and SUVR and Loss Modulus that is approaching significance in the Left Entorhinal cortex. With continued recruitment of subjects with AD and MCI, we hope to expand this method to perform joint analysis of biomechanical, connectomic and pathologic markers in AD patients and bring novel insights in our understanding of the mechanisms of AD onset and progression. We also intend to perform voxel-wise comparisons within brain regions in the future, control for age and sex, as well as include analysis of Tau and Dopamine PET metrics as this study progresses.

Conclusion

Our biomechanical analysis framework has promise to determine correlations between various MRI and PET measures for AD and MCI subjects, providing a physical understanding between tissue mechanics and AD pathophysiology.

Acknowledgements

The authors would like to acknowledge Dr. Veraart (NYU) for providing the MP-PCA denoising algorithm, and support from funding sources P30AG066514 and NIH R21AG071179.

References

1. Double, K. L. et al. Topography of brain atrophy during normal aging and Alzheimer's disease. Neurobiol. Aging 17, 513–521 (1996).

2. Blinkouskaya, Y. & Weickenmeier, J. Spatiotemporal Atrophy Patterns in Healthy Brain Aging and Alzheimer's Disease. in IMECE (2021).

3. Murphy, M. C. et al. Regional brain stiffness changes across the Alzheimer's disease spectrum. NeuroImage Clin. 10, 283–290 (2016).

4. Hiscox, L. V et al. Mechanical property alterations across the cerebral cortex due to Alzheimer's disease. Brain Commun. 2, (2019).

5. Triolo, E. et al. Development and validation of an ultra-high field compatible MR elastography actuator. in Summer Biomechanics, Bioengineering and Biotransport Conference SB3C2021-325 (2021).

6. Triolo, E. R. et al. Design, Construction, and Implementation of a Magnetic Resonance Elastography Actuator for Research Purposes. Curr. Protoc. 2, 1–26 (2022).

7. Karsa, A. & Shmueli, K. SEGUE: A Speedy rEgion-Growing Algorithm for Unwrapping Estimated Phase. IEEE Trans. Med. Imaging 38, 1347–1357 (2019).

8. Maharjan, S. et al. Directional Filter, Local Frequency Estimate and Algebraic Inversion of Differential Equation of Psoas Major Magnetic Resonance Elastography. Open J. Med. Imaging 10, 1–16 (2020).

Figures

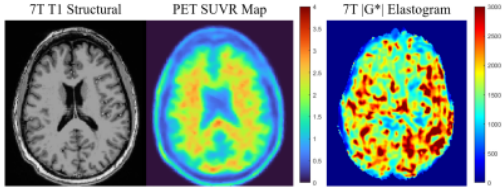

Figure 1: PET SUVR map, to T1, and Elastogram (|G*|, kPa) for the Same Subject in the same image space.

Nucleus	PET SUVR	Storage Modulus (Pa)	Loss Modulus (Pa)
Cerebellar Cortex	0.979 ± 0.049	941.9 ± 72.6	386.8 ± 75.7
Hippocampus	1.355 ± 0.074	1065.7 ± 140.5	396.8± 37.7
Entorhinal	1.167 ± 0.108	861.6 ± 227.0	338.6 ± 176.6
Parietal	1.176 ± 0.053	1034.8 ± 167.4	599.0 ± 202.0
Temporal	1.096 ± 0.050	1026.9 ± 167.9	517.3 ± 115.4
Frontal	1.286 ± 0.127	1018.2 ± 168.3	555.1 ± 172.3
Left Cerebellar Cortex	0.993 ± 0.052	948.7 ± 89.7	364.8 ± 53.0
Left Hippocampus	1.358 ± 0.091	1067.4 ± 142.8	398.3 ± 66.5
Left Entorhinal	1.204 ± 0.146	862.4 ± 243.3	355.1 ± 258.2
Left Parietal	1.211 ± 0.072	1119.4 ± 212.1	644.9 ± 261.2
Left Temporal	1.115 ± 0.057	1066.5 ± 194.1	558.1 ± 151.4
Left Frontal	1.282 ± 0.116	1021.8 ± 182.8	571.2 ± 180.5
Right Cerebellar Cortex	0.967 ± 0.053	948.4 ± 74.0	433.7 ± 114.3
Right Hippocampus	1.361 ± 0.078	1038.4 ± 186.0	383.5 ± 60.4
Right Entorhinal	1.101 ± 0.113	777.7 ± 194.1	292.7 ± 152.0
Right Parietal	1.180 ± 0.054	981.2 ± 145.6	559.1 ± 188.7
Right Temporal	1.096 ± 0.067	939.7 ± 132.4	455.8 ± 87.0
Right Frontal	1.308 ± 0.147	1014.3 ± 150.9	537.9 ± 164.3

Table 1: Average SUVR, Storage Modulus (in Pa), and Loss Modulus (in Pa) for Each Brain Region (Mean ± Standard Deviation). OSS-SNR was also calculated for MRE measures to ensure SNR was high enough for accurate stiffness reconstruction (OSS-SNR > 3).

Nucleus	SUVR & Storage Modulus		SUVR and Loss Modulus	
	R	p-value	R	p-value
Hippocampus	0.4510	0.3694	0.547227	0.2611
Entorhinal	0.7994	0.0563*	0.630394	0.1797
Parietal	0.6142	0.1946	0.5203	0.2900
Temporal	0.4835	0.3313	0.665784	0.1489
Frontal	0.2795	0.5917	0.26924	0.6059
Left Hippocampus	0.4076	0.4224	0.210707	0.6886
Left Entorhinal	0.7724	0.0718*	0.767875	0.0746*
Left Parietal	0.0739	0.8893	0.154204	0.7705
Left Temporal	0.3631	0.4793	0.545053	0.2634
Left Frontal	0.0891	0.8666	0.200306	0.7036
Right Hippocampus	0.5016	0.3107	0.511227	0.3000
Right Entorhinal	-0.4269	0.3986	-0.07232	0.8917
Right Parietal	0.7198	0.1067	0.565237	0.2424
Right Temporal	0.6108	0.1977	0.610555	0.1980
Right Frontal	0.4248	0.4012	0.266453	0.6098

Table 2: Correlation Coefficients and p-values of SUVR and Storage and Loss Modulus for Each Brain Region. While none of the following correlations reach significance, the Entorhinal cortex is approaching significance for Storage Modulus and SUVR (signified by the *). As these subjects are all healthy controls, we do not yet expect to see strong correlations between PET and MRE metrics as we would with AD or MCI subjects.